



Tropical instability waves at 0°N, 23°W in the Atlantic: A case study using Pilot Research Moored Array in the Tropical Atlantic (PIRATA) mooring data

Semyon A. Grodsky, James A. Carton, Christine Provost, Jacques Servain, Joao A. Lorenzzetti, Michael J. Mcphaden

► To cite this version:

Semyon A. Grodsky, James A. Carton, Christine Provost, Jacques Servain, Joao A. Lorenzzetti, et al.. Tropical instability waves at 0°N, 23°W in the Atlantic: A case study using Pilot Research Moored Array in the Tropical Atlantic (PIRATA) mooring data. *Journal of Geophysical Research*, 2005, 110, pp.C08010. <10.1029/2005JC002941>. <hal-00124460>

HAL Id: hal-00124460

<https://hal.science/hal-00124460v1>

Submitted on 12 Jan 2021

HAL is a multi-disciplinary open access archive for the deposit and dissemination of scientific research documents, whether they are published or not. The documents may come from teaching and research institutions in France or abroad, or from public or private research centers.

L'archive ouverte pluridisciplinaire **HAL**, est destinée au dépôt et à la diffusion de documents scientifiques de niveau recherche, publiés ou non, émanant des établissements d'enseignement et de recherche français ou étrangers, des laboratoires publics ou privés.



HAL Authorization

Tropical instability waves at 0°N, 23°W in the Atlantic: A case study using Pilot Research Moored Array in the Tropical Atlantic (PIRATA) mooring data

Semyon A. Grodsky,¹ James A. Carton,¹ Christine Provost,² Jacques Servain,^{3,4}
Joao A. Lorenzetti,⁵ and Michael J. McPhaden⁶

Received 1 March 2005; revised 20 May 2005; accepted 6 June 2005; published 23 August 2005.

[1] Temperature, salinity, velocity, and wind from a mooring at 0°N, 23°W are used along with satellite data for sea surface temperature and sea level to examine the contribution of tropical instability waves (TIWs) to the energy and heat balance of the equatorial Atlantic mixed layer. The TIWs appear as periodic 20–30 day fluctuations of currents, temperature, and salinity, which intensify beginning in June and peak in late boreal summer. The intensification occurs in phase with strengthening of the southeasterly trade winds and the seasonal appearance of the equatorial tongue of cold mixed layer temperatures. In 2002 these waves, which warm the mixed layer by 0.35°C during summer months, are maintained by both barotropic and baroclinic conversions that are of comparable size. Salinity fluctuations, previously neglected, increase the magnitude of baroclinic energy conversion.

Citation: Grodsky, S. A., J. A. Carton, C. Provost, J. Servain, J. A. Lorenzetti, and M. J. McPhaden (2005), Tropical instability waves at 0°N, 23°W in the Atlantic: A case study using Pilot Research Moored Array in the Tropical Atlantic (PIRATA) mooring data, *J. Geophys. Res.*, 110, C08010, doi:10.1029/2005JC002941.

1. Introduction

[2] A tongue of relatively cold water (<25°C) enters the equatorial mixed layer in the eastern Atlantic in late boreal spring in response to intensified winds and a shallowing of the thermocline. This equatorial cold tongue, which plays a central role in the seasonal climate of the tropical Atlantic and eastern Pacific [e.g., Okumura and Xie, 2004], is separated from the warmer waters north of 5°N by a strong narrow temperature front along the North Equatorial Countercurrent. In the mid-1970s, Duing *et al.* [1975] and Legeckis [1977] observed that the meridional position of this temperature front undergoes intraseasonal fluctuations because of tropical instability waves (TIWs) that have 20–30 day timescales and 800–1000 km zonal space scales. The TIWs are now thought to play a key role in the heat budget of the tropical mixed layer [e.g., Hansen and Paul, 1984]. In this paper we present results from a new mooring deployment to examine the TIWs during 2002.

[3] The energy source for TIWs has been linked to instabilities of the mean zonal currents [Philander, 1976]. In general, these waves extract energy through local interactions with the mean current and density fields via barotropic and baroclinic conversions [e.g., Masina *et al.*, 1999]. Discussions of the relative importance of barotropic and baroclinic energy conversions have a long history. Among those emphasizing barotropic processes, Qiao and Weisberg [1995] reported that phase lines associated with TIW velocity variations tilt against the meridional shear of zonal currents, suggesting important barotropic conversions. More detailed observational analyses of Weisberg and Weingartner [1988] and Qiao and Weisberg [1998] and the model simulation study of Jochum *et al.* [2004] also suggest that barotropic instability of the mean zonal currents is the primary local source of energy for TIWs. Johnson and Proehl [2004] have reported substantial correlation of TIW energy with the seasonal and interannual variation in strength of the near-equatorial zonal currents.

[4] While it is generally accepted that current shear (barotropic conversion) is an important source of the TIW energy, controversy exists over partitioning between the barotropic and baroclinic mechanisms. Several observational studies, including those of Hansen and Paul [1984], Luther and Johnson [1990], and Baturin and Niiler [1997], have indicated a greater impact of the baroclinic instabilities on the TIWs. In their model analyses, Masina *et al.* [1999] and Masina [2002] have found a comparable contribution of the barotropic and baroclinic conversions, while McCreary and Yu [1992] have concluded that the baroclinic (frontal) instability is a leading source of the TIW

¹Department of Atmospheric and Oceanic Science, University of Maryland, College Park, Maryland, USA.

²Laboratoire d'Océanographie Dynamique et de Climatologie, Université Pierre et Marie Curie, Paris, France.

³Institut de Recherche pour le Développement, UR 065, Brest, France.

⁴Now at Fundação Cearense de Meteorologia e Recursos Hídricos, Fortaleza, Brazil.

⁵Remote Sensing Division, National Space Research Institute, São José dos Campos, Brazil.

⁶Pacific Marine Environmental Laboratory, NOAA, Seattle, Washington, USA.

energy. Finally, to complicate matters, in his idealized model analysis, *Proehl* [1996] has concluded that the TIWs extract energy from the background state through varying mixes of barotropic, baroclinic, and Kelvin-Helmholtz mechanisms.

[5] One possible explanation for some of the variability among these studies is the fact that some studies, including those of *Weisberg and Weingartner* [1988], *Qiao and Weisberg* [1998], and *Jochum et al.* [2004], do not account for TIW-induced salinity fluctuations. These salinity fluctuations are significant [*McPhaden et al.*, 1984] and could affect the magnitude of the baroclinic conversion, potentially significantly in the central Atlantic, where precipitation associated with the Intertropical Convergence Zone (ITCZ) largely controls the seasonal variations of salinity [*Dessier and Donguy*, 1994] and results in a persistent southward salinity gradient on the equator. Another possible explanation is that different mechanisms come into play under different mean conditions, perhaps explaining the multiple frequency structure observed by *Lyman* [2003] and simulated by *Masina et al.* [1999]. Some observational support has been found in the equatorial Pacific by *Johnson and Proehl* [2004], who demonstrated that TIWs act to reduce both the shear of the large-scale currents and their thermal structure, thus deriving energy from several source mechanisms. They also found that the partitioning between the mechanisms is zonally dependent, with the contribution of the baroclinic conversions from sloping isopycnals increasing westward from 110°W toward the date line.

[6] As mentioned, part of the interest in TIW dynamics lies in their potential contribution to the heat budget of the ocean mixed layer. Estimates of the magnitude of horizontal eddy heat advection of 100 W m^{-2} reported by *Hansen and Paul* [1984], *Bryden and Brady* [1989], *Weingartner and Weisberg* [1991], *Swenson and Hansen* [1999], and *Wang and McPhaden* [1999] are comparable to the seasonal variation of heat flux through the surface. On the other hand, the observational analyses of *Weisberg and Qiao* [2000] and *Wang and Weisberg* [2001] show a strong interplay between the horizontal and vertical components of TIW heat advection, which suggests an out-of-phase relationship between the two. Recently, *Vialard et al.* [2001] and *Jochum et al.* [2004] have questioned the contribution of the TIWs to the mixed layer heat budget altogether. On the basis of modeling studies they suggest that warming by horizontal eddy heat advection is compensated for in part by cooling of the mixed layer by TIW-related entrainment. Previous observational estimates of the impact of TIWs on the mixed layer heat balance that are based on the horizontal component only may thus be overestimated because of the lack of contemporaneous vertical eddy fluxes.

[7] In this paper we evaluate the energetics of the TIWs and their contribution to the seasonal warming of the equatorial cold tongue mixed layer on the basis of analysis of a new mooring data set (temperature, salinity, and velocity) collected at 0°N, 23°W in the tropical Atlantic during the year 2002. In addition to substantially increasing the available moored velocity observations in this basin, the new observation set is enhanced by the availability of a number of additional contemporaneous (mostly satellite)

observations that provide information on spatial fields needed to evaluate the eddy fluxes.

2. Data and Methods

[8] The Pilot Research Moored Array in the Tropical Atlantic (PIRATA) project is an international program (France, Brazil, and United States, <http://www.brest.ird.fr/pirata/pirataus.html>), which maintains a network of surface or near-surface measurements with the principal objective of describing and understanding the evolution of sea surface temperature (SST), upper ocean thermal structure, and air-sea fluxes of momentum, heat, and fresh water in the tropical Atlantic on seasonal to interannual timescales [*Servain et al.*, 1998]. The primary information used in this study comes from a combination of two moorings separated by $\sim 3 \text{ km}$ in the central equatorial Atlantic (0°N, 23°W). At the first mooring, temperature is recorded at 11 depths between 1 and 500 m with 20 m spacing in the upper 140 m, while salinity (via conductivity) is measured at four depths: 1, 20, 40, and 120 m. Wind velocity is measured at 4 m above the sea surface.

[9] At the second mooring an upward looking acoustic Doppler current profiler (ADCP) has provided currents during 1 year (13 December 2001 to 21 December 2002). The PIRATA current meter mooring was deployed in December 2001 from R/V *Atalante* and recovered in December 2002 from R/V *Le Suroit*. The near-surface current meter was an upward looking Workhorse Sentinel acoustic Doppler current profiler (RD Instruments ADCP 300 KHz). The data processing is detailed by *Kartavtseff and Provost* [2003]. The ADCP was located at 130 m depth (between 126.5 and 154.1 m) and provided profiles of the horizontal components of the velocity between 130 and 12 m with a vertical resolution of 4 m and a time step of 1 hour. For the purpose of this study the original time series were averaged and decimated at daily intervals. The velocity data are limited to depths below 12 m because of surface (reflection) effects, but continuous records during the whole observation period are available only between 16 and 120 m depths (see Figures 1a and 1c). The data availability of the temperature and salinity sensors at 0°N, 23°W during the period of interest is shown in Figures 1e and 1f, respectively. The primary observation set used in this analysis is this 1 year long record of daily averaged temperature, salinity, and upward looking ADCP velocity. Although vertical velocity was recorded, because of accuracy considerations, only the horizontal component of velocity is used in this analysis.

[10] In order to evaluate heat and momentum fluxes, observations collected at the buoy site need to be complemented by horizontal gradients of temperature, salinity, and velocity within the mixed layer. Spatial fields of the SST have been provided by Remote Sensing Systems (<http://www.remss.com>). We use 3 day average SST, which is available on a $0.25^\circ \times 0.25^\circ$ grid from the Tropical Rainfall Measuring Mission's Microwave Imager (TMI) aboard the U.S./Japanese Tropical Rainfall Measuring Mission satellite as a proxy for mixed layer temperature. The TMI provides probably the most accurate SST for the tropical oceans because of the advantage of cloud transparency in the microwave band. *Chelton et al.* [2001] have used TMI

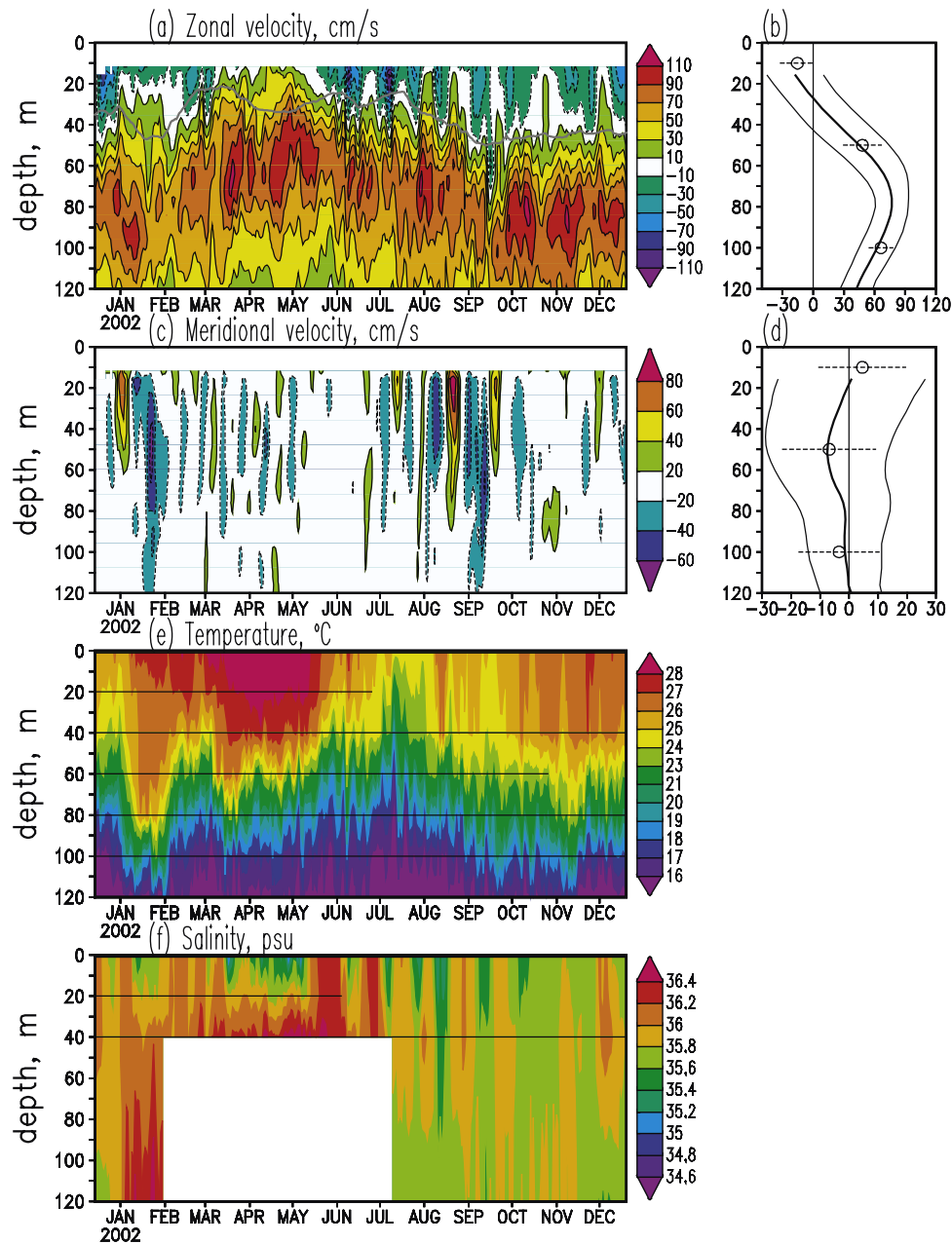


Figure 1. Data from 0°N, 23°W moorings. (a) Zonal and (c) meridional velocity. Gray line in Figure 1a is the mixed layer depth (calculated as the depth where temperature is 1°C below the nighttime sea surface temperature (SST)). Tick marks along the time axes denote the first day of the month. Mean (b) zonal and (d) meridional currents (thick lines). Thin lines in Figures 1b and 1d bound the standard deviation of daily currents. Also shown are mean currents (circles) and standard deviation of currents (horizontal dashes) for 1981 [Weisberg, 1985]. (e) Temperature and (f) salinity from the Pilot Research Moored Array in the Tropical Atlantic (PIRATA) Autonomous Temperature Line Acquisition System (ATLAS) mooring. Horizontal lines in Figures 1e and 1f indicate the data availability at a particular level.

SST to analyze surface signatures of TIWs and discussed applicability of TMI SST for TIW studies. Gentemann *et al.* [2004] have found a negligible bias and a standard deviation of 0.57°C between the TMI SST retrievals and in situ measurements in the tropical Pacific and Atlantic. Comparison of the TMI and PIRATA SSTs at 0°N, 23°W during 2002 shows a standard deviation of the difference of 0.3°C

throughout the year, increasing to 1°C in boreal spring (Figure 2a). During boreal spring the ITCZ is in its southern position, and a decrease in TMI SST accuracy (some differences between TMI and observed SSTs may reach 2°C) is explained by a reduction in data retrievals as the rain-contaminated pixels are disregarded. Fortunately, as the ITCZ shifts southward in boreal spring the SST

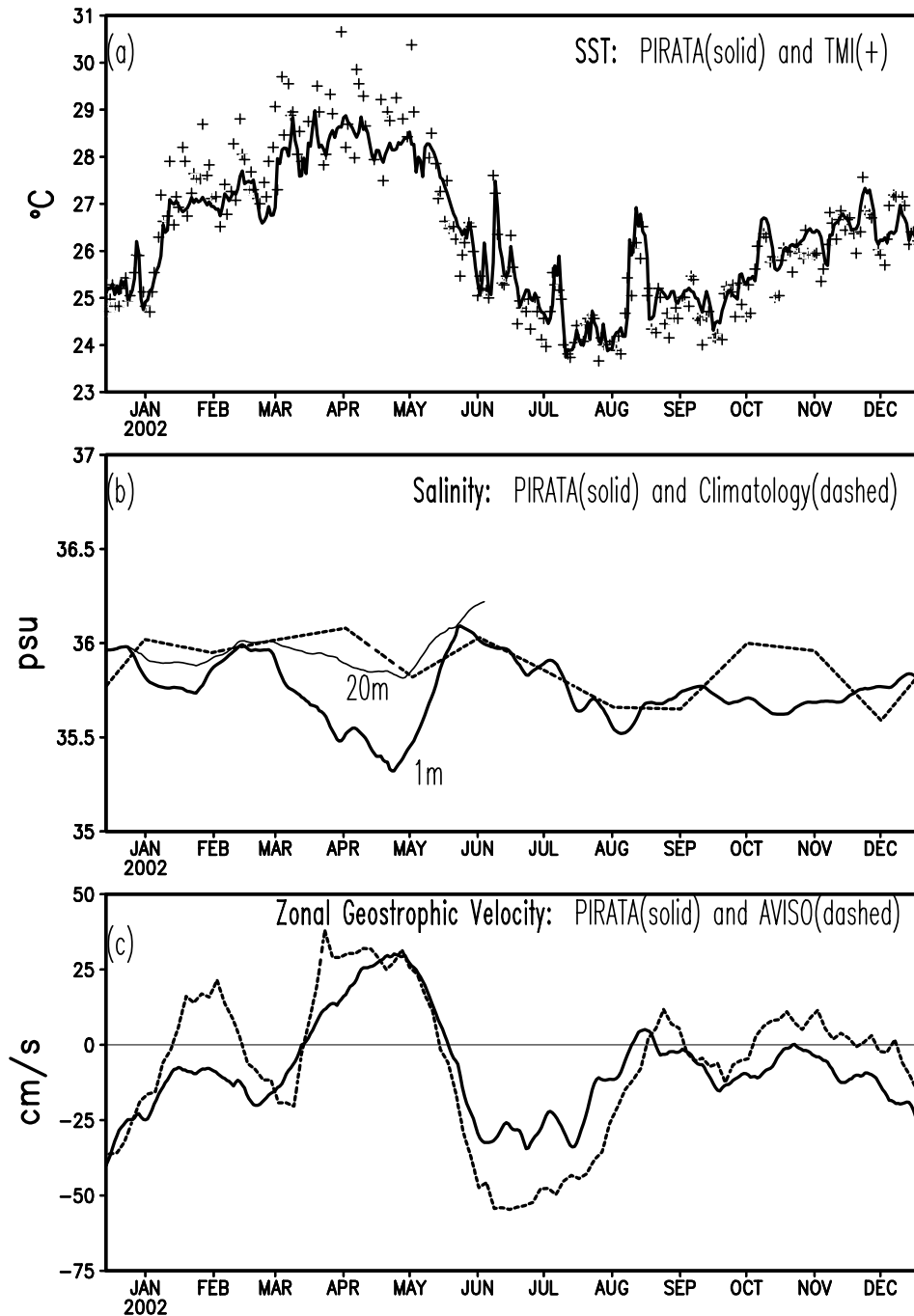


Figure 2. Comparison of (a) PIRATA and the Tropical Rainfall Measuring Mission's Microwave Imager (TMI) 3 day averaged SST, (b) PIRATA monthly running mean salinity at 1 and 20 m depths and climatological monthly surface salinity, and (c) monthly running mean zonal geostrophic currents from PIRATA and Archiving, Validation, and Interpretation of Satellite Oceanographic data (AVISO) altimetry.

gradient weakens, thus decreasing the impact of increasing SST errors on the heat flux and eddy energy flux estimates.

[11] We rely on the climatological monthly estimates of sea surface salinity (SSS) of Dessier and Donguy [1994], available on a $1^\circ \times 1^\circ$ grid. Foltz *et al.* [2004] have shown that the gradient of this climatological SSS provides a reliable estimate of salt advection in the western tropical Atlantic. In the eastern Atlantic, where precipitation asso-

ciated with the ITCZ and African river discharges largely control the seasonal variations of SSS [Dessier and Donguy, 1994], the seasonal variations of the salinity gradient are also well captured by the SSS climatology. These estimates are consistent with PIRATA observations in boreal summer (Figure 2b) but underestimate the near-surface freshening in boreal spring. This underestimation should have little impact on the eddy fluxes estimate because these fluxes are weak during March–May (see section 3).

[12] Computation of near-surface velocity fields also poses a challenge. We use the altimeter-based Archiving, Validation, and Interpretation of Satellite Oceanographic data (AVISO) geostrophic currents, which provide spatial resolution of $0.3^\circ \times 0.3^\circ$ over the tropical oceans at weekly intervals. In the AVISO data (available at <http://las.aviso.oceanobs.com/las/servlets/dataset>), geostrophic zonal velocities at the equator are computed from sea level, η , assuming a balance between the meridional curvature of pressure and the β effect [Picaut *et al.*, 1989; Menkes *et al.*, 1995], $U = -g/\beta \partial^2 \eta / \partial y^2$ (AVISO team, personal communication, 2005), while outside a 5° band around the equator the flow is assumed to be fully geostrophic. Within a 5° band around the equator a connection is computed to ensure continuity with classical geostrophy following Carton and Hackert [1989]. The details of the AVISO current retrieval and data quality assessment have not been published yet. To compare the AVISO currents with the PIRATA measurements, we assume that the near-surface currents can be decomposed into geostrophic and wind-driven components. We estimate the wind-driven component of currents on the equator using the PIRATA wind stress, τ , and the simple frictional model of Cane [1980], in which the friction is parameterized by the Rayleigh linear damping term, $r\mathbf{U}_w$, which balances the wind stress on the equator. In Figure 2c the PIRATA zonal geostrophic currents are calculated by subtracting the wind-driven zonal component, $U_w = \tau_x / \rho r H$, averaged over the upper $H = 40$ m with a frictional timescale, r , and a drag coefficient of 2 days and 1.2×10^{-3} , respectively. Although the discrepancy between the two independent estimates of geostrophic currents is noticeable in January and June, they have similar seasonal variations and capture surfacing of the eastward currents in March–April, westward current strengthening in June (in phase with the onset of TIW season), and relatively weak zonal currents on the equator beginning in August (see also Provost *et al.* [2004] for further comparisons of the PIRATA currents and altimeter data).

[13] Horizontal gradients of temperature, salinity, and velocity are used to estimate the TIW energy balance and TIW-induced heat flux. To evaluate the TIW energy balance, we separate all variables into low- and high-frequency components. Here and throughout the paper a high-frequency component (denoted by a prime) is defined as the deviation from the running mean and is obtained by filtering out the low-frequency component with a running mean rectangular filter whose width, W , will be specified later. The equation for eddy (TIW) energy balance is given by [see, e.g., Brooks and Niiler, 1977]

$$dE/dt = -\rho \langle \mathbf{u}' \cdot (\mathbf{u}' \cdot \nabla \mathbf{U}) \rangle - g \langle \rho' \mathbf{u}' \cdot \nabla_H \rho \rangle / |\rho_z| - \langle \nabla \cdot (\mathbf{u}' p') \rangle, \quad (1)$$

where $E = \rho \langle \mathbf{u}' \cdot \mathbf{u}' \rangle / 2 + g \langle \rho'^2 \rangle / (2|\rho_z|)$. Terms of order three and higher are omitted, and standard notations are used in (1). The subscript H indicates horizontal derivative; angular brackets and the terms without a prime denote running mean.

[14] We are unable to estimate all terms in (1), so we need to rely on a number of simplifying assumptions. The first term on the right-hand side of (1) describes the eddy energy

production by Reynolds stresses acting against the current shear. This term includes the part proportional to the horizontal current shear (barotropic conversion) and the part proportional to the vertical shear (Kelvin-Helmholtz conversion). We neglect the Kelvin-Helmholtz conversion because vertical velocity is not available and because this conversion contributes mainly to daily and shorter fluctuations. We also disregard the barotropic conversion terms involving current derivatives in the zonal direction on the basis of the scaling analysis of Luther and Johnson [1990]. The second term on the right-hand side of (1) describes the eddy energy production by the eddy buoyancy fluxes acting on the density gradient (baroclinic conversion). The third term on the right-hand side of (1) is the pressure work done by eddies. It redistributes the eddy energy spatially and drops out when averaged over the volume [Masina *et al.*, 1999]. Under these simplifications, (1) is written as (2), where only the barotropic conversion due to meridional shear (the first two terms on the right-hand side of (2) and the baroclinic conversion (the second two terms) are retained:

$$dE/dt = -\rho \langle u' v' \rangle U_y - \rho \langle v' v' \rangle V_y - g \langle u' \rho' \rangle \rho_x / |\rho_z| - g \langle v' \rho' \rangle \rho_y / |\rho_z| \quad (2)$$

[15] We average the terms in (2) vertically through the upper 40 m ocean layer, a depth that roughly coincides with the mixed layer depth at the mooring location and spans three upper measurement levels. The vertical density derivative, ρ_z , is then estimated as the central difference between $z = 40$ m and $z = 1$ m levels. Calculations are done for a number of the filter widths, $W = 20$ to 40 days. These multiple calculations give an assessment of the results as a function of the filter width, W .

[16] Meridional shear of the zonal current in (2) is calculated as the sum of geostrophic and wind-driven components, while it is assumed that the meridional divergence is dominated by the wind-driven component. Because of the β effect, even homogeneous wind over the equator produces the meridional divergence, $\partial V_w / \partial y = -\beta \tau_x / (\rho r^2 H)$, and the meridional shear, $\partial U_w / \partial y = \beta \tau_y / (\rho r^2 H)$, assuming the wind-related stress, τ , vanishes at the bottom of the upper $H = 40$ m layer.

[17] The terms in the TIW energy balance equation (2) are estimated as mean values in the upper 40 m ocean layer. Velocity information is available only below 16 m. Because of that we have to make an assumption to relate velocity fluctuations above and below the upper measurement level. Fortunately, an empirical orthogonal function analysis of the velocity data (Figure 3a) shows that neither component varies strongly with depth over the depths for which we have observations. Therefore we assume the velocity fluctuations are depth-independent in the upper 40 m.

[18] A final issue that needs to be addressed is the data dropout in June. During the first half of 2002, all three temperature and salinity sensors in the upper 40 m column were operational, but the 20 m sensors broke in June (Figures 1e and 1f). To account for missing data, a correlation of temperature and salinity variations between $z = 20$ m and $z = 1$ m was calculated using data for other years. This correlation exceeds 0.8, and data scatter around the diagonals, corresponding to equal variations at $z = 1$ m

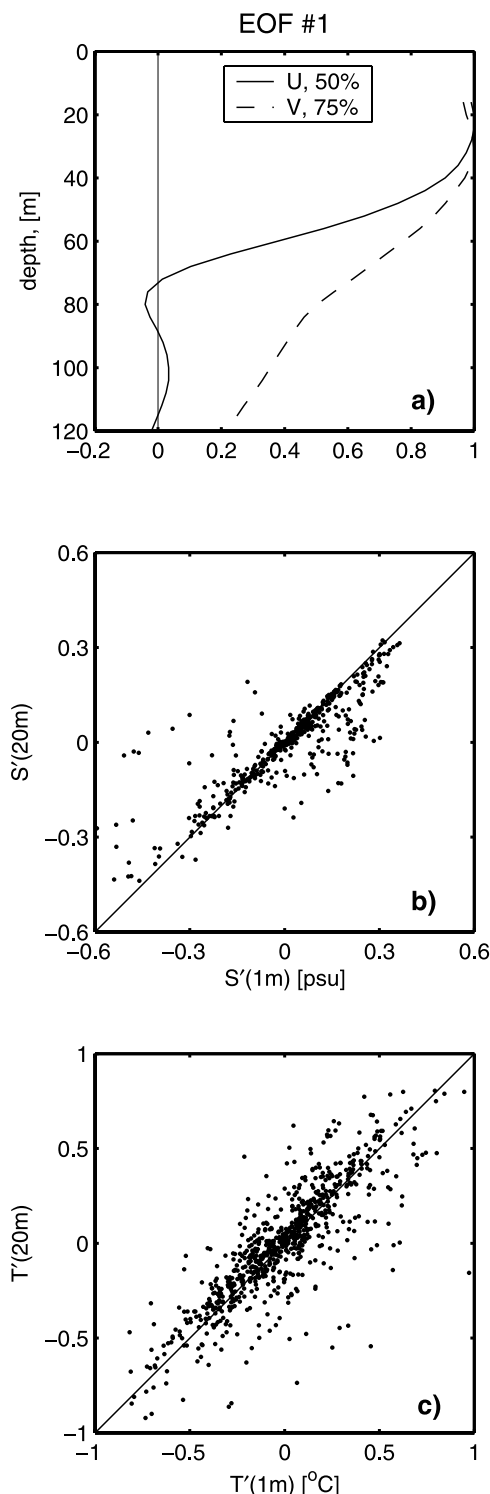


Figure 3. (a) Leading vertical empirical orthogonal function of the intramonth zonal and meridional velocity fluctuations (numbers in the legend are percent of explained variance). (b,c) Comparison of the intramonth fluctuations of salinity and temperature at the near-surface ($z = 1$ m) and mixed layer ($z = 20$ m) horizons.

and $z = 20$ m depths (Figures 3b and 3c). On the basis of this comparison the gap at the 20 m depth was filled using the 1 m observations.

3. Results

[19] We begin by examining the background velocity observed at 0°N , 23°W (Figures 1a and 1c). The velocity record for the year 2002 shows a modest westward flowing South Equatorial Current (SEC) with a mean current of $\sim 20 \text{ cm s}^{-1}$ at 16 m depth (Figure 1b). The SEC is present within the 30–50 m depth mixed layer except in boreal spring. Below the mixed layer in the thermocline, there is an intense eastward flowing Equatorial Undercurrent (EUC), whose mean velocity is 80 cm s^{-1} (Figure 1b), that may exceed 110 cm s^{-1} at ~ 80 m depth (Figure 1a). In boreal spring, in response to the easterly wind weakening, the EUC shallows, causing the appearance of eastward currents along with warm temperatures in the mixed layer (Figures 1a and 1e). Shallowing of the EUC increases the salinity of the lower mixed layer (Figure 1f), but in the upper 20 m, increased precipitation leads to freshening.

[20] In contrast to the seasonal zonal currents the meridional currents at 0°N , 23°W are dominated by intraseasonal variations (Figure 1c), with a mean southward flow from $z = 16$ m to 80 m (Figure 1d). This southward flow is highest, 8 cm s^{-1} , just below the mixed layer at 50 m depth. Both zonal and meridional mean currents and their standard deviations are similar to that reported for the year 1981 by Weisberg [1985] at 0°N , 28°W (Figures 1b and 1d).

[21] In boreal summer the intraseasonal oscillations of meridional velocity, which are present year-round, strengthen. Interestingly the meridional velocity fluctuations vary coherently throughout the upper 120 m of the water column (vertical coherence in the 20–40 day band exceeds 0.6), while the zonal velocity fluctuations are coherent only within the mixed layer. Fluctuations in zonal velocity are largest in June–July, while fluctuations in meridional velocity are largest in August–September (Figures 1a and 1c). These intraseasonal velocity fluctuations are accompanied by pronounced fluctuations of salinity at the buoy location (Figure 1f), while the intraseasonal fluctuations of temperature are less evident (Figure 1e). These fluctuations of temperature occur approximately 2 months later in the year than fluctuations previously observed at 0°N , 28°W during the year of 1983 by Weisberg and Weingartner [1988], indicating that the seasonal phase of the TIWs can vary significantly in the Atlantic.

[22] During June–September, five TIW events are evident in Figure 4. These events result from the arrival of TIW crests, which propagate westward at phase speed $40 \pm 4 \text{ cm s}^{-1}$, as estimated from the longitude/time diagram of the TMI SST at 2°N (plus/minus bounds the scatter in speed of individual TIWs). At 16 m depth the summertime velocity fluctuations typically consist of a southward anomaly of 0.5 m s^{-1} and a westward surge of comparable magnitude (see Figures 4c and 4d), suggesting the NE–SW orientation of the velocity fluctuation ellipses. For the five TIW events in June–September the horizontal velocity components fluctuate almost in phase. Cross-correlation analysis of the horizontal velocity fluctuations during June–September (not shown) indicates that the

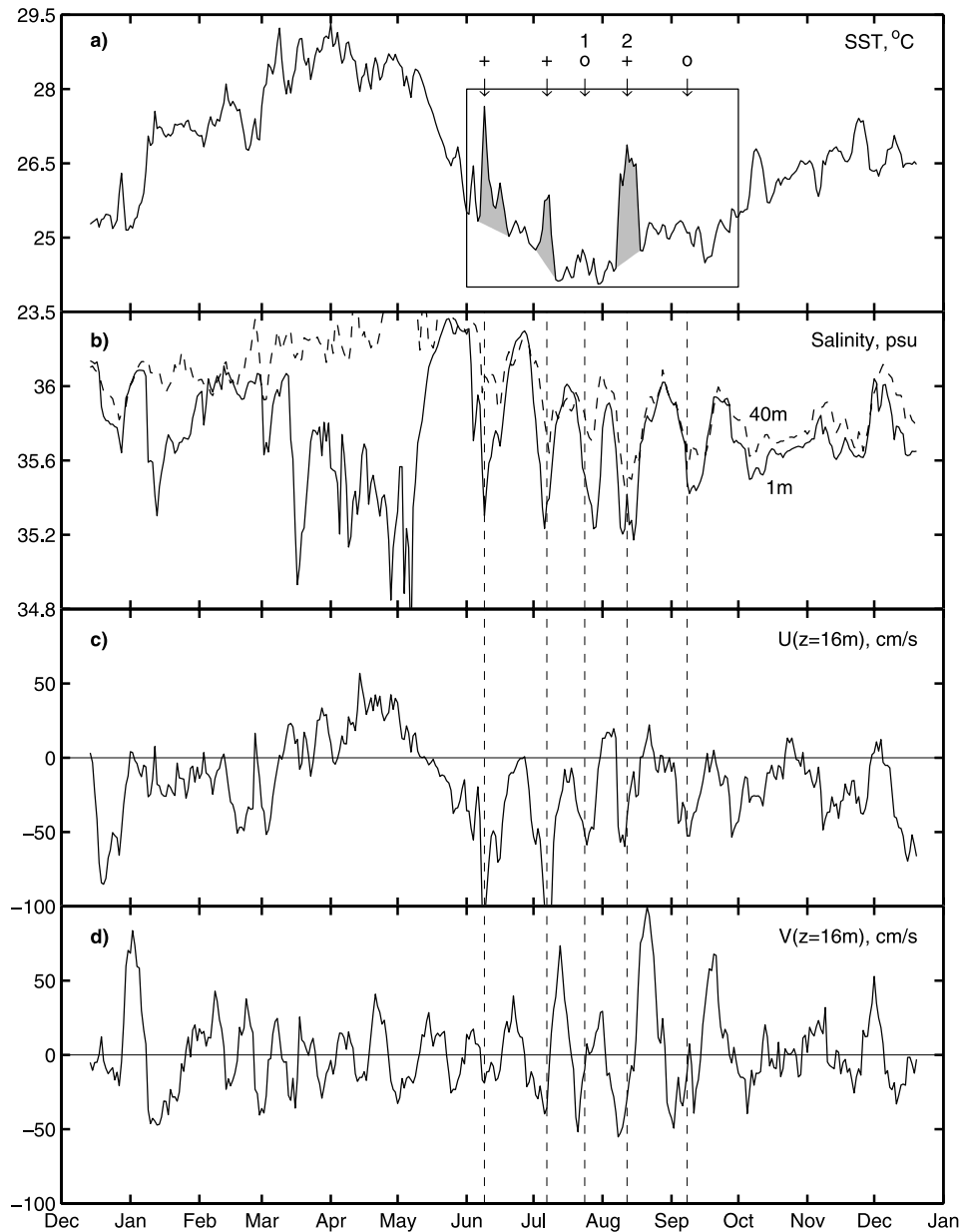


Figure 4. (a) SST, (b) sea surface and 40 m depth salinity, (c) zonal currents at 16 m depth, and (d) meridional currents. Westward current surges during June–September are marked with arrows. Crosses and circles mark events with stronger and weaker SST response, respectively. Numbers mark events illustrated in Figure 8.

meridional component, v' , slightly leads the zonal component, u' , by ~ 3 days.

[23] Salinity throughout the mixed layer varies in phase with changes in meridional velocity (Figures 1c, 1f, 4b, and 4d), apparently determined by meridional excursions of the seasonal salinity gradient (fresher water to the north) due to TIWs. Temperature fluctuations are also evident in the summer months (Figure 4a); however, they are not as well correlated with meridional velocity fluctuations and thus contribute less to the meridional eddy buoyancy flux (hence baroclinic conversion). During the 4 month period (June–September) a succession of five TIW events takes place. Increases in temperature at the mooring site occur

for three of the five TIW events, with an average increase of $\sim 2^\circ\text{C}$. During the other two (indicated by circles in Figure 4a), there was essentially no local temperature increase.

[24] We next consider temporal changes of the TIWs beginning with the eddy kinetic energy (Figure 5a). Zonal velocity covariance peaks in June–July, leading by a month the peak in meridional covariance that occurs in August. The Reynolds stress increases in magnitude in June (Figure 5b), following the strengthening of the cyclonic meridional shear of the zonal currents in May, and remains high until September (Figure 5c). The Reynolds stress is mostly confined to the mixed layer and the upper

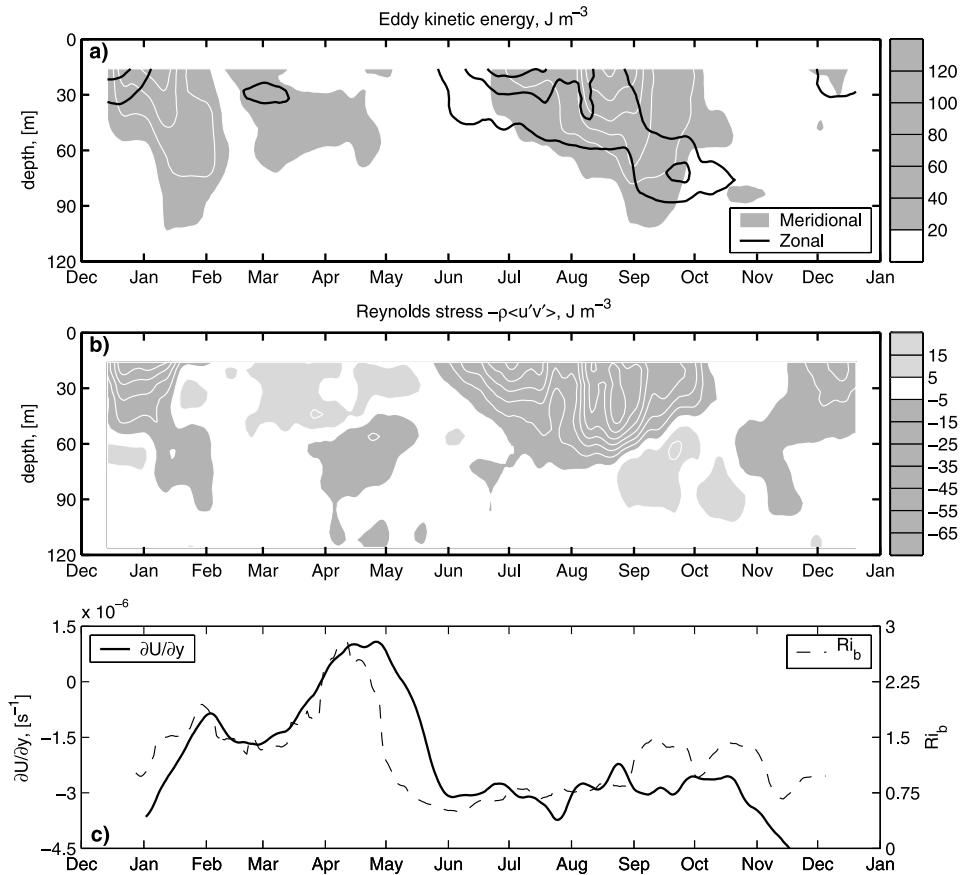


Figure 5. (a) Eddy kinetic energy of the zonal and meridional components. Isolines are drawn at 20 J m^{-3} intervals. Meridional component values exceeding 20 J m^{-3} are shaded. (b) Reynolds stress. Isolines are drawn at 10 J m^{-3} intervals. Values greater than 5 J m^{-3} or less than -5 J m^{-3} are in light and dark gray shading, respectively. (c) Meridional shear of the zonal current and bulk Richardson number.

thermocline, confirming that the energy transfer is occurring at these depths.

[25] To evaluate the importance of Kelvin-Helmholtz instability to the energy budget of the TIWs we estimate the bulk Richardson number, Ri_b , on the basis of the PIRATA temperature, salinity, and velocity measurements in the mixed layer and the depth of the core of the EUC. Throughout the year, Ri_b remains larger than the critical value of 0.25, suggesting a minor (if any) impact of the Kelvin-Helmholtz instability on the TIW energy budget.

[26] Barotropic energy conversion occurs in response to cyclonic shear of the mean zonal currents (Figure 6a). This term is positive in boreal summer and increases again in boreal winter. It dominates eddy energy dissipation produced by the meridional velocity divergence.

[27] Next we consider the impact of salinity observations on the baroclinic energy conversion estimate. Accounting for salinity affects the magnitude of baroclinic conversion in two ways: by affecting the background density gradient and by affecting the buoyancy flux. Salinity fluctuation occurs in phase with velocity fluctuation (Figure 4), hence contributing to the buoyancy flux. To estimate the effect of salinity on the magnitude of baroclinic conversions, we first begin with the estimate of density fluctuation, ρ' , and background density gradient, $\nabla_H \rho$, on the basis of the

temperature only. This approach may underestimate the buoyancy flux, $-g\langle \rho' u' \rangle$, given differences in TIW-induced fluctuation of temperature and salinity (Figures 4a and 4b), and may also underestimate the background isopycnal slope. If salinity fluctuations are neglected in the evaluation of the baroclinic conversion terms, the zonal, $-g\langle u' \rho' \rangle \rho_x / |\rho_z|$, and meridional, $-g\langle v' \rho' \rangle \rho_y / |\rho_z|$, components almost cancel each other (Figure 6b), as has been found previously by *Weisberg and Weingartner* [1988]. When salinity is included, however, the meridional term increases substantially, thus unbalancing the terms and increasing the magnitude of the total baroclinic conversion. As a result, the baroclinic conversion becomes comparable in size to the barotropic conversion (Figure 6c). The small effect of salinity on the zonal component of the baroclinic conversion is explained in part by the horizontal salinity gradient, which is primarily meridional [*Dessier and Donguy*, 1994] in the eastern equatorial Atlantic and hence has little impact on the background zonal density gradient.

[28] We next consider the contribution of the TIWs to the seasonal mixed layer heat budget. Increases in temperature at the buoy site occur for three of the five TIW events (marked by crosses in Figure 4a), with an average increase of 2°C (Figure 4). During the other two (marked by circles), there was essentially no local temperature increase. To understand differences in SST response to

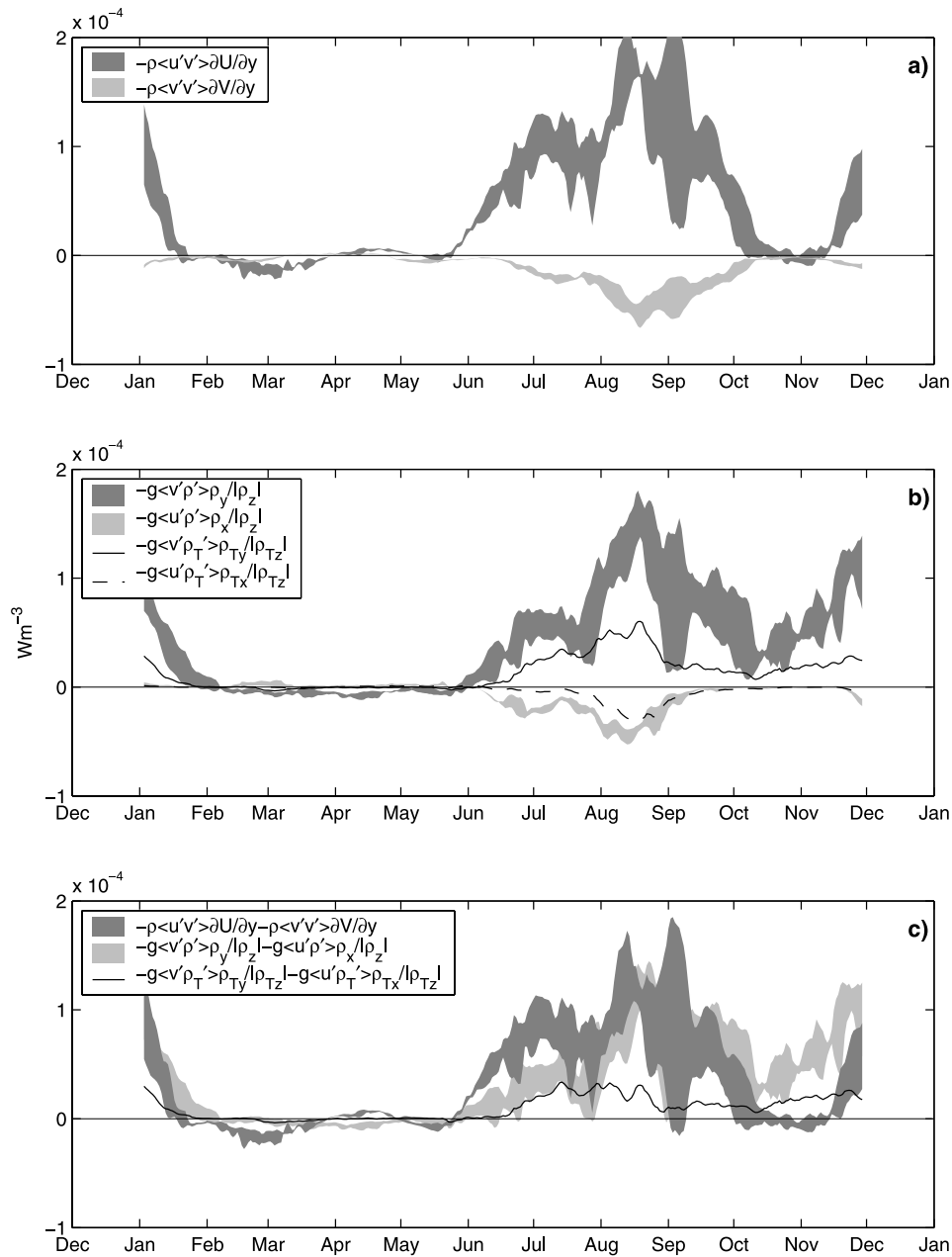


Figure 6. (a) Barotropic energy conversion averaged through the upper 40 m. Shadings bound the spread of estimates on the basis of 20, 30, and 40 day running means. (b) Same as in Figure 6a but for baroclinic conversion. Lines present estimates (marked with subscript “T” in the legend) on the basis of temperature-only data computed with 30 day running mean. (c) Comparison of the combined barotropic and baroclinic conversions.

individual TIW events, we turn our attention to horizontal heat advection, which is the scalar product of the gradient of mixed layer temperature and horizontal velocity. Heat advection is an important term of the heat balance of the equatorial mixed layer. *Wang and Weisberg* [2001] have found that in the central Pacific, roughly half of the SST variation at intraseasonal timescales is accounted for by heat advection. At the buoy location we compare the 3 day mean rate of change of the mixed layer heat content and heat advection (Figure 7) and find that the advection term

accounts for 52% of the heat content variance, in close agreement with the previous estimate.

[29] To assess differences in heat advection for individual TIWs, we compare the geographic orientation of the mixed layer velocity and the thermal front during two events (see Figure 4a for numbering). During these two events the magnitude of the velocity fluctuations are similar (Figures 4c and 4d), but the temperature fluctuations differ substantially. Overlaying the velocity on the SST fields we find in Figure 8a that the velocity fluctuation is

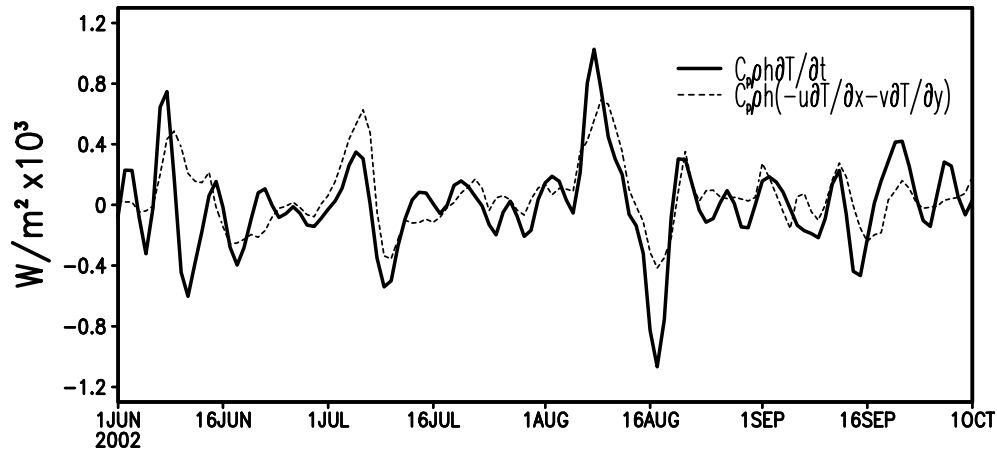


Figure 7. Three day averaged rate of change of the mixed layer heat content and horizontal heat transport.

oriented parallel to isotherms during event 1. Moreover, the buoy is located within the equatorial cold tongue where the SST gradient is weaker in comparison to the northern edge of the cold tongue. Under these conditions, as in event 1, warming is weak (see Figures 4a and 8a). In contrast, during event 2 the mixed layer temperature gradient is

almost northward, while the currents are southwestward (Figure 8b). During event 2 the buoy is at the northern edge of the equatorial cold tongue, where the magnitude of the SST gradient is larger than in the interior of the cold tongue. In this case, temperature advection is large and warming at the mooring site is significant.

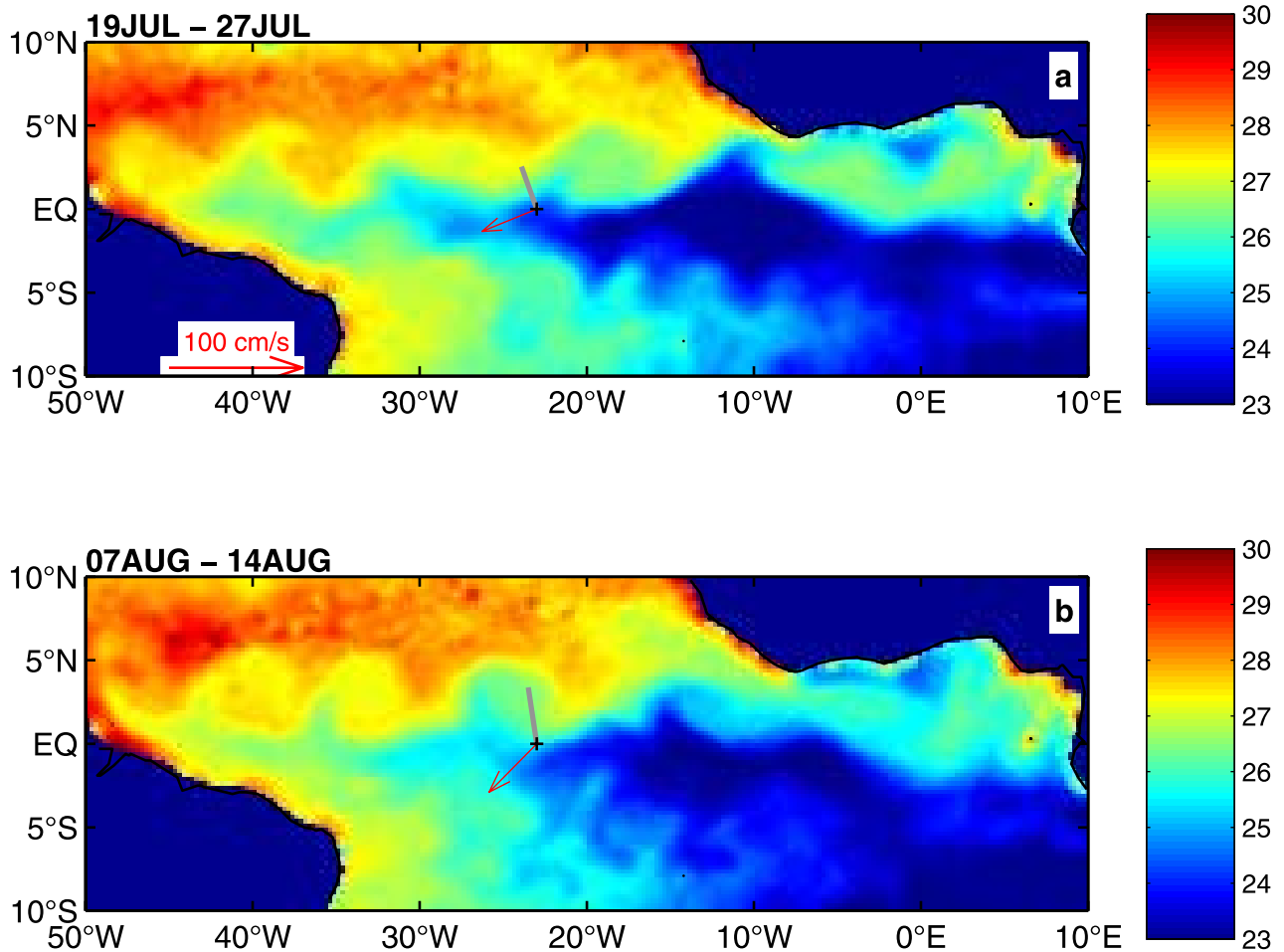


Figure 8. Tropical Atlantic SST (in °C) during (a) late July and (b) early August. Arrows and gray lines show currents at $z = 16$ m and direction of SST gradient, respectively.

[30] In contrast to the southward surges of events 1 and 2, northward surges cause SST to drop to the temperature of the equatorial cold tongue, and so the gradient of temperature becomes weak. This asymmetry allows velocity fluctuation to induce substantial eddy horizontal heat advection, $-C_p \rho H \langle \mathbf{u}' \cdot \nabla T' \rangle$. In the present study we find eddy horizontal heat advection of the order of 100 W m^{-2} in the upper $H = 50 \text{ m}$, in line with previous studies [see, e.g., Weisberg and Weingartner, 1988]. This strong horizontal eddy heat advection may be balanced by vertical eddy flux convergence or by a mixed layer warming tendency. We evaluate the seasonal warming due to individual TIWs, comparing the SST to the value it would have in the absence of TIWs, as estimated by the linear interpolation of SST between the beginning and end of each TIW warm event (shown in Figure 4a). We assume that the TIWs affect SST only during the warm events (shaded). The seasonal average of SST is higher during boreal summer by 0.35°C when we include the shaded regions in the average versus if we did not. Thus the increase in seasonal SST due to the TIWs is 0.35°C , translating into a convergence of eddy heat flux of 10 W m^{-2} in the upper 50 m. This estimate of heat storage rate is very much less than direct estimates of the horizontal eddy heat advection [see, e.g., Weisberg and Weingartner, 1988]. Together these case results are in accord with the conclusion of Vialard *et al.* [2001] and Jochum *et al.* [2004], who suggest that cooling due to vertical eddy heat advection compensates for warming due to horizontal eddy heat advection, and the net impact of the TIWs on the heat budget of the equatorial mixed layer is weak.

4. Summary

[31] The TIWs appear as periodic 20–30 day fluctuations in currents which develop beginning in June in phase with the strengthening of the southeasterly trades and the seasonal appearance of cool ($<24^\circ\text{C}$) mixed layer temperatures along the equator. We use temperature, salinity, and velocity time series from two moorings, both located at 0°N , 23°W , for 1 year (December 2001 to December 2002) along with complementary satellite and climatological data to evaluate some of the features of tropical instability waves, including the barotropic and baroclinic conversions in the TIW energy budget, and assess the role of TIWs in the mixed layer heat balance in this region of the equatorial Atlantic.

[32] We begin by examining the phase relationship among variables. Zonal current fluctuations are stronger in June–July, while meridional fluctuations persist throughout the year, reaching their maximum in August–September. Fluctuations of both current components are of similar amplitude (0.5 m s^{-1}). The meridional velocity fluctuations vary coherently throughout the upper 120 m (the whole water column of ADCP observations), while the zonal velocity fluctuations are coherent only within the mixed layer. These vertical structures are very similar to those for instability waves of similar periods in the central Pacific at 0°N , 140°W [McPhaden, 1996]. Some, but not all, of the fluctuations result in fluctuations of the mixed layer temperature. In contrast, fluctuations of mixed layer salinity are well correlated with fluctuations of current and occur in phase with the meridional velocity fluctuations.

[33] We next consider the TIW energy budget. We find that accounting for observed salinity fluctuations (neglected in some previous studies) increases our estimate of baroclinic energy conversion by a factor of three. As a result, we find barotropic and baroclinic conversions are similar in magnitude, suggesting that both maintain the TIWs in the central equatorial Atlantic during boreal summer.

[34] Finally, we consider the contribution of TIWs to the seasonal heat budget. The summer contribution of the TIWs to the warming of the mixed layer is found to be quite small (10 W m^{-2}). This modest storage rate is very much less than estimates of previous studies of the summer contribution of TIWs to convergence of horizontal eddy heat flux. This inconsistency indicates that the vertical eddy heat advection must balance horizontal eddy heat advection, thus reducing the impact of TIWs on the heat budget of the equatorial cold tongue.

[35] **Acknowledgments.** Data management is conducted by the TAO project office at NOAA/PMEL in collaboration with many research institutes listed on the PIRATA web site (<http://www.pmel.noaa.gov/pirata>). This work was supported by the French Ministry of Research (ACI Climat), NOAA's office of Oceanic and Atmospheric Research and office of Global Programs, the National Science Foundation, the Institut de Recherche pour le Développement, Centre National de Recherche Spatiale, Météo-France, Institut National des Sciences de l'Univers Convention N01CV071, and National Space Research Institute, Brazil. The ADCP mooring opportunity was the result of French–Brazilian cooperation within the PIRATA project. The ADCP data were processed and validated at Laboratoire d'Océanographie Dynamique et de Climatologie (Paris). The ADCP data are available at http://www.pmel.noaa.gov/tao/data_deliv/deliv-pir.html. We deeply acknowledge the help of the Lanoissellé family and crew members from R/V *Atalante* and R/V *Le Suroit* for mooring construction, deployment, and recovery. We are grateful to M. Jochum, formerly of MIT, J. Lyman of NOAA/PMEL, and anonymous reviewers for comments on the original manuscript. TMI/SST data are produced by Remote Sensing Systems. The altimeter products were produced by SSALTO/DUACS and distributed by AVISO, with support from CNES, France.

References

- Baturin, N. G., and P. P. Niiler (1997), Effects of instability waves in the mixed layer of the equatorial Pacific, *J. Geophys. Res.*, **102**, 27,771–27,793.
- Brooks, I. H., and P. P. Niiler (1977), Energetics of the Florida Current, *J. Mar. Res.*, **35**, 163–191.
- Bryden, H., and E. C. Brady (1989), Eddy momentum and heat fluxes and their effect on the circulation of the equatorial Pacific Ocean, *J. Mar. Res.*, **47**, 55–79.
- Cane, M. (1980), On the dynamics of the equatorial currents, with application to the Indian Ocean, *Deep Sea Res., Part A*, **27**, 524–544.
- Carton, J. A., and E. C. Hackert (1989), Application of multi-variate statistical objective analysis to the circulation in the tropical Atlantic Ocean, *Dyn. Atmos. Oceans*, **13**, 491–515.
- Chelton, D. B., S. K. Esbensen, M. G. Schlax, N. Thum, M. H. Freilich, F. J. Wentz, C. L. Gentemann, M. J. McPhaden, and P. S. Schopf (2001), Observations of coupling between surface wind stress and sea surface temperature in the eastern tropical Pacific, *J. Clim.*, **14**, 1479–1498.
- Dessier, A., and J. R. Donguy (1994), The sea surface salinity in the tropical Atlantic between 10°S and 30°N —Seasonal and interannual variations (1977–1989), *Deep Sea Res., Part I*, **41**, 81–100.
- Duing, W., P. Hisard, E. Katz, J. Meincke, L. Miller, K. V. Moroshkin, G. Philander, A. A. Ribnikov, K. Voit, and R. Weisberg (1975), Meanders and long waves in equatorial Atlantic, *Nature*, **257**, 280–284.
- Foltz, G. R., S. A. Grodsky, J. A. Carton, and M. J. McPhaden (2004), Seasonal salt budget of the northwestern tropical Atlantic Ocean along 38°W , *J. Geophys. Res.*, **109**, C03052, doi:10.1029/2003JC002111.
- Gentemann, C. L., F. J. Wentz, C. A. Mears, and D. K. Smith (2004), In situ validation of Tropical Rainfall Measuring Mission microwave sea surface temperatures, *J. Geophys. Res.*, **109**, C04021, doi:10.1029/2003JC002092.
- Hansen, D., and C. Paul (1984), Genesis and the effect of long waves in the equatorial Pacific, *J. Geophys. Res.*, **89**, 10,431–10,440.

- Jochum, M., P. Malanotte-Rizzoli, and A. Busalacchi (2004), Tropical instability waves in the Atlantic Ocean, *Ocean Modell.*, **7**, 145–163.
- Johnson, E. S., and J. A. Proehl (2004), Tropical instability wave variability in the Pacific and its relation to large-scale currents, *J. Phys. Oceanogr.*, **34**, 2121–2147.
- Kartavtseff, A., and C. Provost (2003), Mouillages courantométriques PIRATA Décembre 2001–Décembre 2002, *Rapp. Interne LODYC 2003–01*, 128 pp., Univ. Pierre et Marie Curie, Paris.
- Legeckis, R. (1977), Long waves in eastern equatorial Pacific Ocean—View from a geostationary satellite, *Science*, **197**, 1179–1181.
- Luther, D. S., and E. S. Johnson (1990), Eddy energetics in the upper equatorial Pacific during the Hawaii-to-Tahiti shuttle experiment, *J. Phys. Oceanogr.*, **20**, 913–944.
- Lyman, J. M. (2003), Separating 20 and 30 day tropical instability waves in the central Pacific, *Eos Trans. AGU*, **84**(52), Ocean Sci. Meet. Suppl., Abstract OS51K-01.
- Masina, S. (2002), Instabilities of continuously stratified zonal equatorial jets in a periodic channel model, *Ann. Geophys.*, **20**, 729–740.
- Masina, S., S. G. H. Philander, and A. B. G. Bush (1999), An analysis of tropical instability waves in a numerical model of the Pacific Ocean: 2. Generation and energetics of the waves, *J. Geophys. Res.*, **104**, 29,637–29,662.
- McCreary, J. P., and Z. Yu (1992), Equatorial dynamics in a $2^{1/2}$ -layer model, *Prog. Oceanogr.*, **29**, 61–132.
- McPhaden, M. J. (1996), Monthly period oscillations in the Pacific North Equatorial Countercurrent, *J. Geophys. Res.*, **101**, 6337–6359.
- McPhaden, M. J., M. Fieuz, and J. Gonella (1984), Meanders observed in surface currents and hydrography during an equatorial Atlantic transect, *Geophys. Res. Lett.*, **11**, 757–760.
- Menkes, C., J.-P. Boulanger, and A. J. Busalacchi (1995), Evaluation of TOPEX and basin-wide Tropical Ocean and Global Atmosphere—Tropical Atmosphere Ocean sea surface topographies and derived geostrophic currents, *J. Geophys. Res.*, **100**, 25,087–25,099.
- Okumura, Y., and S. P. Xie (2004), Interaction of the Atlantic equatorial cold tongue and the African monsoon, *J. Clim.*, **17**, 3589–3602.
- Philander, S. G. H. (1976), Instabilities of zonal equatorial currents, *J. Geophys. Res.*, **81**, 3725–3735.
- Picaut, J., S. P. Hayes, and M. J. McPhaden (1989), Use of geostrophic approximation to estimate time-varying zonal currents at the equator, *J. Geophys. Res.*, **94**, 3228–3236.
- Proehl, J. A. (1996), Linear stability of equatorial zonal flows, *J. Phys. Oceanogr.*, **26**, 601–621.
- Provost, C., S. Arnault, N. Chouaib, A. Kartavtseff, L. Bunge, and E. Sultan (2004), Equatorial pressure gradient in the Atlantic in 2002: TOPEX Poseidon and Jason versus the first PIRATA current measurements, *Mar. Geod.*, **27**, 13,774–13,769.
- Qiao, L., and R. H. Weisberg (1995), Tropical instability wave kinematics: Observations from the Tropical Instability Wave Experiment, *J. Geophys. Res.*, **100**, 8677–8693.
- Qiao, L., and R. H. Weisberg (1998), Tropical instability wave energetics: Observations from the Tropical Instability Wave Experiment, *J. Phys. Oceanogr.*, **28**, 345–360.
- Servain, J., A. J. Busalacchi, M. J. McPhaden, A. D. Moura, G. Reverdin, M. Vianna, and S. E. Zebiak (1998), A Pilot Research Moored Array in the Tropical Atlantic (PIRATA), *Bull. Am. Meteorol. Soc.*, **79**, 2019–2031.
- Swenson, M. S., and D. V. Hansen (1999), Tropical Pacific Ocean mixed layer heat budget: The Pacific cold tongue, *J. Phys. Oceanogr.*, **29**, 69–81.
- Vialard, J., C. Menkes, J.-P. Boulanger, P. Delecluse, E. Guilyardi, M. J. McPhaden, and G. Madec (2001), A model study of oceanic mechanisms affecting equatorial Pacific sea surface temperature during the 1997–98 El Niño, *J. Phys. Oceanogr.*, **31**, 1649–1675.
- Wang, C. Z., and R. H. Weisberg (2001), Ocean circulation influences on sea surface temperature in the equatorial central Pacific, *J. Geophys. Res.*, **106**, 19,515–19,526.
- Wang, W., and M. J. McPhaden (1999), The surface layer heat balance in the equatorial Pacific Ocean, part I: Mean seasonal cycle, *J. Phys. Oceanogr.*, **29**, 1812–1831.
- Weingartner, T. J., and R. H. Weisberg (1991), A description of the annual cycle in sea surface temperature and upper ocean heat in the equatorial Atlantic, *J. Phys. Oceanogr.*, **21**, 83–96.
- Weisberg, R. H. (1985), Equatorial Atlantic velocity and temperature observations—February–November 1981, *J. Phys. Oceanogr.*, **15**, 533–543.
- Weisberg, R. H., and L. Qiao (2000), Equatorial upwelling in the central Pacific estimated from moored velocity profilers, *J. Phys. Oceanogr.*, **30**, 105–124.
- Weisberg, R. H., and T. J. Weingartner (1988), Instability waves in the equatorial Atlantic Ocean, *J. Phys. Oceanogr.*, **18**, 1641–1657.

J. A. Carton and S. A. Grodsky, Department of Atmospheric and Oceanic Science, University of Maryland, 224 Computer and Space Science Building, Room 2409, College Park, MD 20742, USA. (senya@atmos.umd.edu)

J. A. Lorenzetti, Remote Sensing Division, INPE, Avenida Astronautas, 1758, 12227-010 São José dos Campos, SP, Brazil.

M. J. McPhaden, Pacific Marine Environmental Laboratory, NOAA, 7600 Sand Point Way NE, Seattle, WA 98115, USA.

C. Provost, Laboratoire d’Océanographie Dynamique et de Climatologie, Université Pierre et Marie Curie, 4, place Jussieu, F-75252 Paris Cedex 5, France.

J. Servain, FUNCEME, Avenida Rui Barbosa, 1246, 60115-121 Fortaleza, CE, Brazil.